PCCP

RSC Publishing

PAPER

View Article Online
View Journal | View Issue

Effects of O_2 pressure on the oxidation of VO_x/Pt(111)

Cite this: *Phys. Chem. Chem. Phys.*, 2013, **15**, 12124

Zhenyan Tang, Shaolin Wang, Lihua Zhang, Ding Ding, Mingshu Chen* and Huilin Wan

Vanadium oxide (VO_x) has been extensively used in many oxidation and selective oxidation reactions. In this study, VO_x thin films were prepared in an ultra-high vacuum (UHV) chamber by evaporating V onto a Pt(111) surface followed by subsequent oxidation at 623 K in 1×10^{-7} Torr O_2, and further oxidized in the 'high-pressure' reaction cell with 1 Torr O_2. The film quality and structure were investigated by high-resolution electron energy loss spectroscopy (HREELS), X-ray photoelectron spectroscopy (XPS), low energy electron diffraction (LEED), low energy ion scattering spectroscopy (LEIS), Auger electron spectroscopy (AES), and *in situ* infrared reflection absorption spectroscopy (IRAS). On the Pt(111) surface, VO_x forms isolated O═VO_x (x = 0–3) species, surface two-dimensional (2D) (2×2)-V_2O_3 domains, a bi-layer structure with a $(3\sqrt{3} \times 6)$ arrangement, and a complicated tri-layer structure as the coverage increases from submonolayer to multilayer. Under the UHV conditions, the oxidation state of V is mainly +3 and the stability was found to be surface V_2O_3 > bi-layer V_2O_3 > tri-layer one. After exposing to 0.3–1 Torr O_2, VO_x can be oxidized to higher oxidation states, mainly V_2O_5, as evidenced by the shifts of the core-level binding energies and presence of V═O. These results indicate that thorough oxidation of VO_x requires sufficiently high O_2 pressure, and that vanadium-based catalysts may possess higher oxidation states under most reaction conditions in the presence of O_2.

Received 15th February 2013,
Accepted 15th April 2013

DOI: 10.1039/c3cp50712b

www.rsc.org/pccp

Introduction

The interesting physical and chemical properties of vanadium oxides, originated from a variety of vanadium oxidation states and coordinated oxygen species, have inspired numerous studies in the past several decades.[1–13] Moreover, vanadium oxide has been widely used in heterogeneous catalysis, particular in oxidation and dehydrogenation of alkanes,[14–22] and also in the oxidation of SO_2 to SO_3 (ref. 23) and the selective catalytic reduction (SCR) of nitric oxides.[24,25] The broad applications of vanadium oxide make it an interesting model system to study the influence of the surface structure on the catalytic properties. Understanding the detail structures and oxidation states of vanadium oxides on a molecular level is the key factor in designing more efficient catalysts. Such studies should provide very useful information for designing highly efficient catalysts.[22]

Thin films of vanadia have been studied on several well-defined metal oxide surfaces like TiO_2(110),[26–30] Al_2O_3,[6,7,31,32] CeO_2,[21,33–36] and many metal crystal surfaces.[9,34–50] These studies provided opportunities for better understanding the relationships between the structures and catalytic activities, and the promotion effects of the supports. Especially, on single crystal metal surfaces, well-defined vanadia thin films can be grown. Somorjai's group[36] prepared an ordered $(\sqrt{3} \times \sqrt{3})$ R30°-V_2O_3 film on a Au(111) surface by depositing vanadium followed by subsequent oxidation. Kishi and Fujiwara[37,38] reported that a V_2O_3-like oxide phase formed on Cu(100) when oxidized at room temperature and ordered VO(111)-like structures formed on both the Cu(100) and Ni(110) surfaces oxidized at 523 K. Well-ordered V_2O_3(0001) films with vanadyl groups were grown on W(110) and Au(111).[3,4,39] Well-ordered V_2O_5(001) thin films on Au(111) were prepared by oxidation of the vanadia in 38 Torr O_2 and used as a model surface to investigate the catalytic reactivity for partial oxidation of methanol.[39–41] Thin films of vanadium oxides on Pd(111)[42–47] and Rh(111)[8,48–51] have also been studied in detail. Literature reported results showed that the structures and properties of vanadia thin films were affected significantly by the substrate surface and thickness. It had been shown that a NaCl-type VO film and VO_x ($0.8 \leq \times \leq 1.3$) epitaxial films can be grown on the Pt(111) surface by evaporating vanadium in a controlled water background (8×10^{-10} Torr).[52]

One of the key issues for partial oxidations over the supported vanadium-based catalysts is which oxygen species, V═O, V–O–V, or V–O-support, is the most active or selective

State Key Laboratory of Physical Chemistry of Solid Surfaces, National Engineering Laboratory for Green Chemical Productions of Alcohols-Ethers-Esters, Department of Chemistry, College of Chemistry and Chemical Engineering, Xiamen University, Xiamen 361005, Fujian, China. E-mail: chenms@xmu.edu.cn; Fax: +86-592-2183047; Tel: +86-592-2183723

oxygen species. In our serial work, we first selected the Pt(111) surface as the substrate to grow model vanadia surfaces, regarding that the bulk Pt is stable under the most catalytic reaction conditions and relatively simple in vibrational spectroscopies as compared to oxide supports. The vanadia thin films were grown by depositing vanadium onto the Pt(111) surface in UHV followed by subsequent oxidation. Well-ordered monolayer and bi-layer films were found to form at one and two monolayers, respectively. Isolated vanadyl ($O{=}VO_x$) forms at submonolayer, and a third attached layer formed at 2 ML $< \theta <$ 3 ML. The effects of the 'high pressure' oxygen on these films were examined and discussed.

Experimental

The experiments were carried in two ultra-high vacuum (UHV) chambers with a base pressure of 5×10^{-10} Torr. One equipped with a high-resolution electron energy loss spectrometer (HREELS, LK-5000), an elevated-pressure reactor furnished with an *in situ* infrared reflection absorption spectroscope (IRAS), low-energy electron diffraction (LEED), and an Auger electron spectrometer (AES). The HREELS measurements were performed in a specular reflection geometry $\ominus_{in} = \ominus_{out} = 35^\circ$ with a primary energy of 7.254 eV and a typical resolution of $\sim$2 meV. The AES data were acquired with a primary beam energy of (2.5 keV). The second chamber was equipped with an X-ray photoemission spectrometer (XPS) and a low energy ion scattering spectrometer (LEIS) (Thermo Multilab 2000). XPS measurements were performed using Al Kα (1486.6 eV) and a hemispherical analyzer with a 10 μm diameter sample collection area. LEIS was done using 1 keV He^+ generated in a hot cathode ion gun, directed at the sample with a 45° angle of incidence, and a pass energy of 50 eV.

The Pt(111) sample was mounted with a Ta wire that is heated resistively. A C-type (W-5%Re/W-26%Re/W) thermocouple was spot-welded on the backside of the sample. The sample was cleaned by repeated Ar^+-sputtering and subsequent annealing at 1100 K in UHV. The sample may be heated at 800 K in O_2 to remove carbon contamination before being annealed at 1100 K in UHV. The cleanness of the Pt(111) sample was confirmed by AES/LEED and XPS. Vanadium was deposited under UHV from a resistively heated tantalum filament wrapped with high purity vanadium wire (99.999%). The coverage of one monolayer (ML) was defined from the break-point obtained from the plot of AES or XPS V/Pt ratio *versus* the deposition time, in which a single atomic layer of oxide film was supposed to cover the whole substrate surface. This was also confirmed by the LEIS and HREELS measurements using CO as a probe. High purity CO (Hong Kong Specialty Gases Co., Ltd.) was further purified by a liquid nitrogen trap before being introduced into the chamber and the sample was kept at room temperature during CO adsorption experiment.

Results and discussion

The vanadia thin films were prepared by depositing V onto the Pt(111) surface at room temperature in UHV followed by subsequent oxidation at 623 K in 1×10^{-7} Torr O_2 for 10 min. The AES ratio of V/Pt as a function of the V deposition time is displayed in Fig. 1(A). Two break-points are evidenced at 15 and 30 min. This demonstrates a layer-by-layer growth model. The amount of VO_x at the deposition time of 15 min was defined as one monolayer (1 ML), which corresponds to a full cover of the Pt(111) surface by a one atomic layer of VO*x*. The full cover of the Pt(111) surface at the first breakpoint was confirmed by LEIS (Fig. 1(B)), which is a surface-sensitive technique, acquiring information from the topmost one atomic layer.[53] As shown in Fig. 1(B), with an ion beam energy of 1000 eV, the O, V and substrate Pt are peaked at 430, 730, and 910 eV, respectively. At submonolayer, scattering from the surface Pt atoms are still observed; while at and above one monolayer, no Pt signal is detected.

HREELS was applied to characterize the vanadium oxide thin films. Fig. 2 shows HREEL spectra for the VO_x/Pt(111) with VO_x coverages of 0.3–1.0 ML. For coverages below 0.5 ML, the phonon features of the VO_x/Pt(111) consist in a strong loss peak at 128 meV, which can be attributed to the stretching vibration of the vanadyl group ($V{=}O$).[3,45] Concurrently, there appears a weak loss peak at 94–96 meV probably related with the V–O–Pt vibration and a weak peak at around 61 meV corresponding to

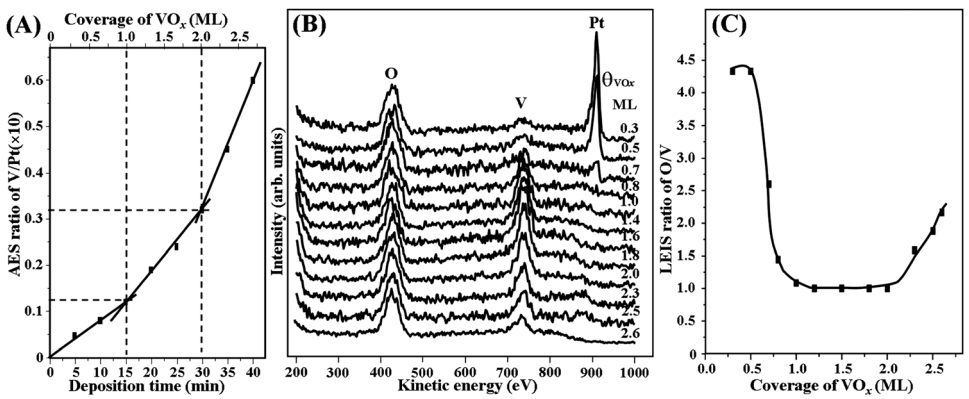

Fig. 1 (A) V/Pt AES ratios as a function of the deposition time; (B) LEIS spectra for the VO_x /Pt(111); (C) O/V LEIS ratios as a function of the VO_x coverage.

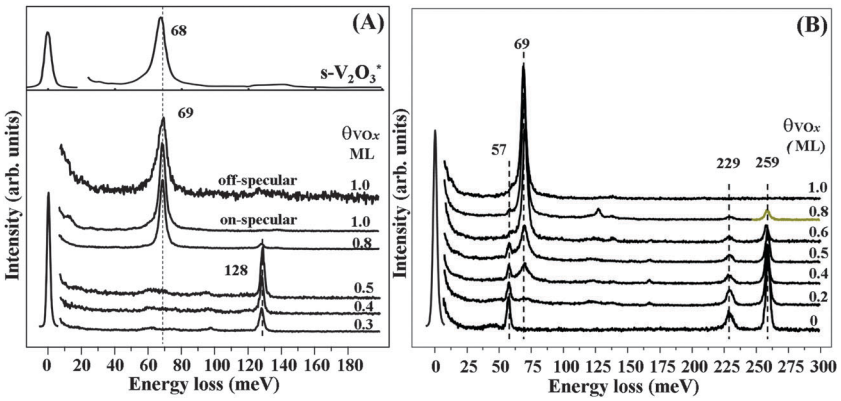

Fig. 2 (A) HREEL spectra for the VO_x/Pt(111) with VO_x coverages of 0.3–1 ML. The coverages of VO_x were indicated in the figure. A spectrum of the 1 ML-V_2O_3 on Pd(111)[45] was compared at the top panel. (B) HREEL spectra for the VO_x/Pt(111) with saturated adsorption of CO at room temperature.

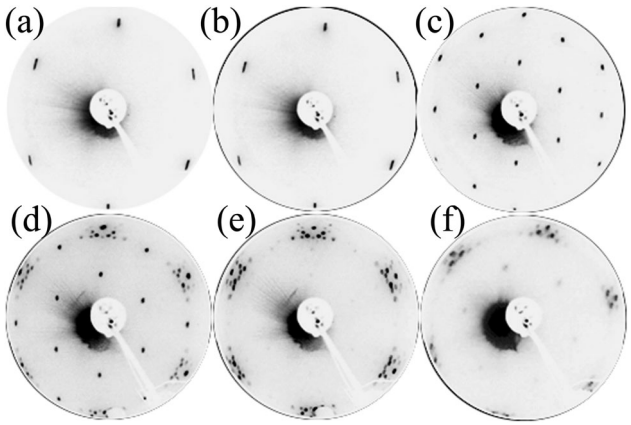

Fig. 3 LEED patterns of the VO_x/Pt(111) surfaces: (a) clean Pt(111) at 63 eV, (b) 0.5 ML VO_x/Pt(111) at 63 eV, (c) 1 ML VO_x/Pt(111) at 58 eV, (d) 1.3 ML VO_x/Pt(111) at 51 eV, (e) 2 ML VO_x/Pt(111) at 53 eV, (f) 2.5 ML VO_x/Pt(111) at 63 eV.

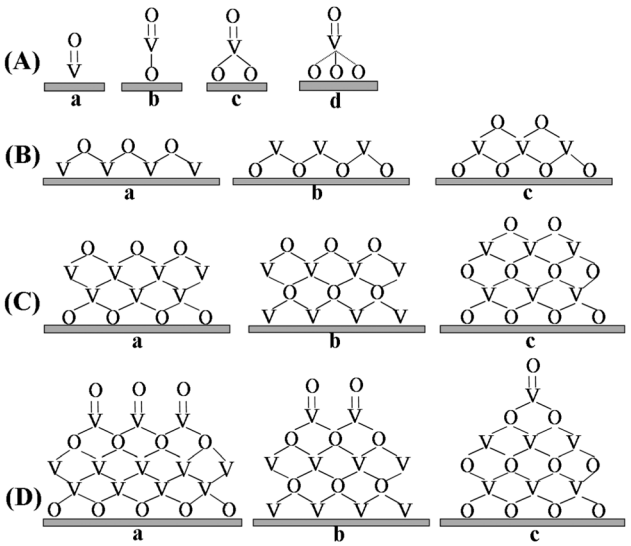

Fig. 4 Structure models (side-view) for the VO_x/Pt(111) at coverages of (A) 0.3–0.5 ML, (B) 1 ML, (C) 2 ML, and (D) 3 ML.

Pt–O species on the uncovered Pt surface.[54] The 0.5 ML VO_x/Pt(111) surface still exhibits a (1×1) LEED pattern with respect to the Pt(111) substrate (Fig. 3(a) and (b)). These results suggest that the VO_x on Pt(111) may form O═VO_x (x = 0–3) as an isolated species or small incommensurate domains that are randomly located on the surface, as shown in Fig. 4(A).

As the VO_x coverage continuously increases above 0.5 ML, a phonon peak at 69 meV appears and becomes dominant, while the loss peak at 128 meV fades away. Simultaneously, a (2×2) LEED pattern appears. At 1 ML, there is only one phonon loss at 69 meV, and exhibits a sharp (2×2) LEED pattern (Fig. 3c). These results evidence the formation of a well-ordered surface structure. There are three possible arrangements of the O and V atoms, O–V–Pt, V–O–Pt and O–V–O–Pt, as shown in Fig. 4(B)–a, b, and c, respectively, among which a and b should have only one phonon feature associated with oxygen, while c should have at least two phonon losses. To clarify this uncertainty, the off-specular HREEL spectrum which provides for both the perpendicular and parallel vibrational modes was measured and compared in Fig. 2A. There is no new loss feature appeared in the off-specular spectrum, confirming that in the 1 ML VO_x/Pt(111) there is only one vibrational mode that oxygen involves. Hence the stacking sequence of O–V–O–Pt in Fig. 4(B)–c can be excluded. Regarding that, a single loss feature of 68 meV and a (2×2) LEED pattern were also observed for the 1 ML VO_x/Pd(111).[45,46] The 1 ML VO_x/Pd(111) was proposed to be a surface V_2O_3, noted as s-V_2O_3, in which the V atoms bond directly with the surface Pd atoms and oxygen atoms locate on the topmost bonding with the V atoms and forming V–O–V bridges.[45,46] The single phonon mode at 69 meV and a (2×2) LEED pattern observed for the 1 ML VO_x/Pt(111) suggest a surface structure resembling that of the 1 ML V_2O_3/Pd(111). That is a surface V_2O_3 formed on the Pt(111) surface with V atoms bonding directly to the surface Pt atoms and oxygen atoms on the top layer forming V–O–V bridges, as indicated in Fig. 4(B)–a. The FeO/Pt(111) was also proposed to have a O–Fe–Pt arrangement.[55]

CO was used to probe the growth of VO_x on Pt(111), as shown in Fig. 2B. On the clean Pt(111) surface, two ν_{CO} loss

peaks of 259 and 229 meV and a loss peak of 57 meV assigned to the Pt–C vibrations are observed, respectively.[56] Exposing VO_x/Pt(111) surface to CO at room temperature appear similar ν_{CO} loss features as on the clean Pt(111), the intensity of which decreases as the VO_x coverage increases up to 1 ML. However, the loss features corresponding to VO_x change significantly, *i.e.* 128 to 69 meV, especially for those with VO_x coverages less than 0.5 ML. And a (2 × 2) LEED pattern appears instead of the (1 × 1). Such results reveal that the O═VO_x(x = 0–3) species at low coverage is isolated on the surface and compressed into 2D surface V_2O_3 domains upon coadsorption with CO.

Fig. 5 shows HREEL spectra for one to multi-layer VO_x films on the Pt(111) surface. At 1 ML, the loss peak at 69 meV is characteristic of a s-V_2O_3. Above 1 ML, a new loss peak at 62 meV appears, sacrificing the intensity of the loss peak at 69 meV. This change completes as the VO_x coverage increases up to 2 ML. At the same time new LEED spots corresponding to a $(3\sqrt{3} \times 6)$ pattern appear (Fig. 3D), and become sharp and solely at 2 ML (Fig. 3E). Such a LEED pattern was observed for 0.8 MLE TiO_x on Pt(111), and named as a zigzag-like structure.[57] The apparently different LEED patterns for the 1 and 2 ML films conclude that the second VO_x layer is not epitaxial on the first layer, but reconstructs to a different arrangement. The phonon feature of 62 meV was also observed for a porous (2 × 2)-V_2O_3 phase obtained by reducing a (4 × 4) V_5O_{14}/Pd(111) surface[47] and for a reduced 0.25 MLE Rh(111)-$(\sqrt{7} \times \sqrt{7})$R19.1° VO_x.[48] The phonon loss peak at 62 meV is broader comparing to the loss peak at 69 meV (Fig. 5). It should consist of at least two phonon features. Based on the above information, three possible structures, O–V–V–O–Pt, O–V–O–V–Pt and O–V–O–V–O–Pt, were proposed in Fig. 4(C)–a, b and c, respectively. In the s-V_2O_3 (Fig. 4(B)–a), the oxidation state of the V is +3. In the structures of O–V–O–V–Pt and O–V–O–V–O–Pt (Fig. 4(C)–b and c), the oxidation states for the V atoms in the upper layer should be higher than +3 since those V atoms bond with more oxygen atoms as compared to that in O–V–Pt structure (Fig. 4(B)–a). A higher loss energy of the loss peak related with V–O–V would be encountered.[58,59] Therefore, the O–V–O–V–Pt and O–V–O–V–O–Pt structural models can be excluded regarding that loss peak shifts from 69 to 62 meV. Surnev[44] also reported that the growth of additional adlayers on the s-V_2O_3, *i.e.* a O–V–O–V–Pt model, was not favored. Here, another structural model of O–V–V–O–Pt was proposed. Since the electronegativity of Pt is higher than that of V, the charging amount of the V atoms in the upper layer for the O–V–V–O–Pt (Fig. 4(C)–a) would be less than that for the O–V–Pt (Fig. 4(B)–a). Hence, a lower loss energy is expected for this V–O–V species. This is consistent with the experimental observation of the shift of loss energy from 69 to 62 meV.

For coverage exceeding 2 ML (Fig. 5), the phonon peak of 128 meV corresponding to the V═O appears again together with a phonon at 90 meV, while the phonon at 62 meV maintains. This suggests that the third layer may attach weakly on the second layer, consistent with the layer-by-layer growth of VO_x as seen from the AES break-point (Fig. 1(A)). This is also supported by the top surface layer information obtained by LEIS (Fig. 1(B) and (C)). Note again that LEIS is a surface-sensitive technique in probing the topmost layer of a solid surface.[53] As the VO_x coverage increases from submonolayer to 1 ML, the ratio of the O/V LEIS intensities continuously decreases to a constant value at 1 ML which maintains up to 2 ML (Fig. 1(C)). The initial decrease of the O/V ratio should be contributed to the surface chemisorbed oxygen on the Pt substrate surface. The constant value for 1 ML to 2 ML reveals that the surface composition should be similar for surfaces of 1 ML and 2 ML. Above 2 ML, the O/V LEIS ratio increases quickly, suggesting the formation of a high oxygen involved topmost surface. This is consistent with the HREELS results that a strong loss peak at 128 meV appears above 2 ML, *i.e.* an oxygen terminated V═O species located on the topmost layer. The LEED pattern becomes complicated.

The thermal stability of the VO_x/Pt(111) surfaces with different thicknesses was investigated by annealing at various temperatures. When the 0.4 ML VO_x/Pt(111) surface was annealed above 673 K, the isolated O═VO_x(x = 0–3) species networked to the surface V_2O_3 domains as evidenced by the disappearance of the 128 meV phonon and the appearance of the 69 meV phonon (Fig. 6A) and a (2 × 2) LEED pattern. This reveals that the isolated O═VO_x(x = 0–3) species bonds weakly and is mobile on the Pt(111) surface, consistent with the results observed in coadsorption with CO. For a 1 ML VO_x/Pt(111) surface, the phonon features, as well as the LEED patterns, do not change upon annealing between 623 and 773 K, as shown in Fig. 6B. The 2 ML VO_x/Pt(111) surface is stable up to 673 K, but decomposes gradually when annealed at 723 K, as evidenced by the shift of the phonon peak from 62 to 69 meV and the decrease of the V/Pt AES ratio (Fig. 6(C)). Annealing the 2.5 ML VO_x/Pt(111) surface at above 673 K observes weakening of the V═O loss peak at 128 meV, as well as a quick decrease of the V/Pt AES ratio to a value of about 0.036, corresponding to a bilayer structure. Further annealing at higher temperature, a sharp loss peak at 69 meV occurs, and the AES ratios of

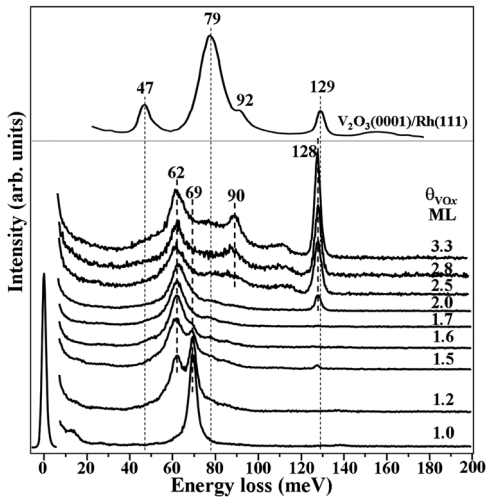

Fig. 5 HREEL spectra for the VO_x/Pt(111) with a coverage range of 1.0–3.3 ML. A bulk-like V_2O_3 spectrum was compared at the top.[49]

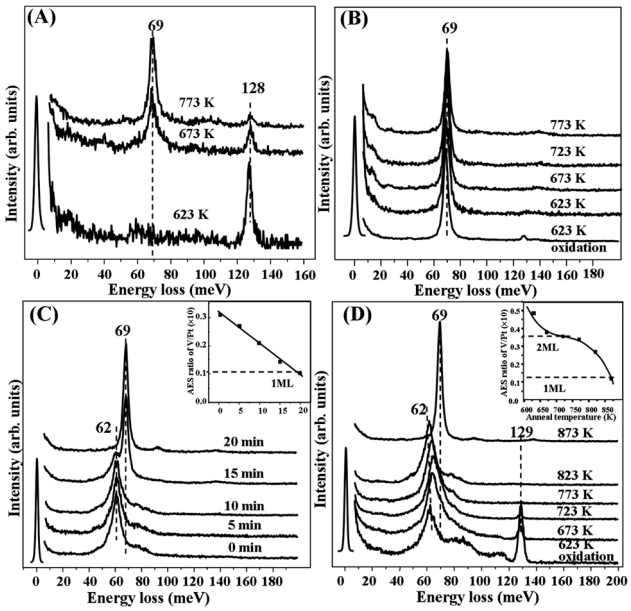

Fig. 6 HREEL spectra of the VO_x/Pt(111) samples annealed at different temperatures or different times. (A) 0.4 ML, (B) 1 ML, (C) 2 ML annealed at 723 K with different times, (D) 2.5 ML. The insets show the AES ratios as a function of the annealing time or temperature.

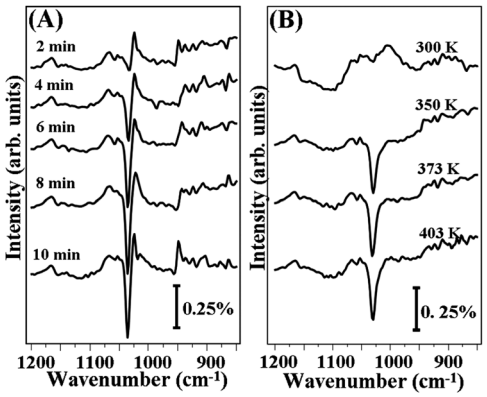

Fig. 8 IRAS spectra for (A) the 0.9 ML VO_x/Pt(111) exposed to 1 Torr O_2 at room temperature, (B) 3 ML VO_x/Pt(111) exposed to 1 Torr O_2 at the indicated temperatures.

V/Pt also decreases to 0.012, consistent with the decomposition of the bilayer structure to a s-V_2O_3. These results clearly demonstrate the relative stability to be 1 ML > 2 ML > multi-layer VO_x/Pt(111).

The above results show that VO_x only reaches a low oxidation state under UHV conditions. In fact, they are stable even at O_2 pressure of 5×10^{-5} Torr. It is then interesting to examine them near the real catalytic reaction conditions. The sample was transferred into the 'high pressure' reaction cell that was connected to the UHV chamber. High purity O_2 was filled up to 1 Torr, and the sample was heated to a certain temperature for 10 min. After pumping out the O_2, the sample was moved back to the UHV chamber at room temperature for HREELS measurements. The results are compared in Fig. 7. For the 0.9 ML VO_x/Pt(111) (Fig. 7(A)), the main loss feature is 128 meV and some weak peaks at 80 ~ 120 meV after exposing to 1 Torr O_2. Note that loss features at 150–200 meV may be due to some contamination. The significant changes of the loss features indicate oxidation of the (2×2)-V_2O_3/Pt(111) to O═VO_x as shown by the insert in Fig. 7(A), which are more obviously seen for the 3 ML VO_x/Pt(111) sample (Fig. 7(B)). The broad loss peaks at 80–120 meV and a sharp peak at 128 meV can be assigned to a bulk-like V_2O_5 surface.[60] These results conclude that the V_2O_3 films stable in UHV are further oxidized at the higher pressure of O_2.

In fact, when the 0.9 ML VO_x/Pt(111) is exposed to 1 Torr O_2 at room temperature, a vibration peak at 1038 cm^{-1} corresponding to the V═O vibration appears,[3,45] as seen from the IRAS spectra in Fig. 8(A). This intensity peak increases with the exposure time, and reaches stability at an exposure time of 10 min. The appearance of V═O confirms the oxidation of V_2O_3/Pt(111), as shown by the inserts in Fig. 7(A). For the 3 ML VO_x/Pt(111), the V═O species forms at 343–373 K (Fig. 8(B)) upon exposing to 1 Torr O_2.

X-Ray photoelectron spectroscopy (XPS) is a powerful technique to determine the oxidation state of an element. However, it is a little bit difficult for vanadium oxides, since the shifts of the binding energies for the different oxidation states are small

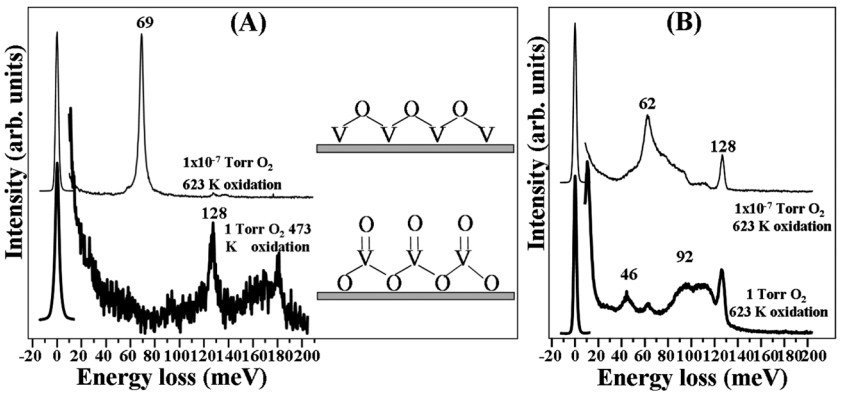

Fig. 7 HREEL spectra of the VO_x/Pt(111) samples before and after exposing to 1 Torr O_2. (A) 0.9 ML, (B) 3 ML.

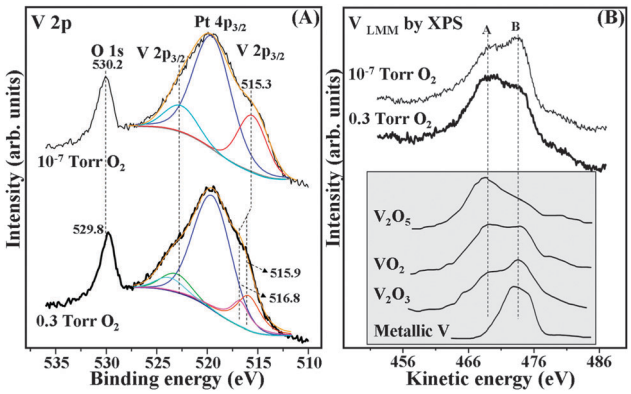

Fig. 9 XP spectra of a 3 ML VO_x/Pt(111). (A) V2p and O1s; (B) AES of V_{LMM} obtained by XPS excitation, and AES lines from ref. 61 were shown in the insert. The film was oxidized in 1×10^{-7} Torr O_2 at 623 K, or in 0.3 Torr O_2 at 623 K as indicated in the figures.

as compared to the full width at half maximum (FWHM).[61] The XPS spectra of the 3 ML VO_x/Pt(111) film oxidized at 10^{-7} and 0.3 Torr O_2 are compared in Fig. 9. Since the two V 2p peaks ($2p_{3/2}$ and $2p_{1/2}$) overlap with the Pt $4p_{3/2}$ peak, peak fittings were performed to better evaluate the difference of the oxidation states as shown in Fig. 9(A), and the parameters for each peak were summarized in Table 1. Here we notice that for the film oxidized at 1×10^{-7} Torr O_2, the $V2p_{3/2}$ shows a broad peak (FWHM = 3.4 meV) at 515.3 eV, which can be attributed to V_2O_3.[44,48,61] This is consistent with HREELS results as discussed above. After oxidation at 0.3 Torr O_2, the V $2p_{3/2}$ peaks shift to higher binding energies, and can be decomposed into two peaks, 515.9 eV for V^{4+} and 516.8 eV for V^{5+}.[27,40,61–65] In contrast, the O 1s peak shifts to a lower binding energy, from 530.2 to 529.8 eV, which is characteristic of a higher oxidation state.

V Auger lines ($L_{23}M_{23}M_{45}$) excited by X-ray are more sensitive to the changes of the oxidation states of vanadium.[61] Regarding the overlap of the Pt $4p_{3/2}$ and V $2p_{3/2}$, V $2p_{1/2}$ peaks, the V Auger lines were also used to evaluate the oxidation state of the VO_x thin films, as shown in Fig. 9(B). The low kinetic energy side, marked as A at 468.2 eV, originates from the O 2p position of the valence band; and the high kinetic energy side, marked as B at 473.4 eV, is the d-band emission close to the Fermi level.[61] The Auger line shape for the VO_x/Pt(111) oxidized at 10^{-7} Torr O_2 (uper line in Fig. 9(B)) is very similar to that of V_2O_3 reported in ref. 61 as shown in the insert of Fig. 9(B). Moreover, the HREELS and LEED results also confirm to be a V_2O_3 thin film. After oxidation at 0.3 Torr O_2, the line shape (lower line in Fig. 9(B)) characterizes a mixture of VO_2 and V_2O_5,[61] consistent with the results from XPS V 2p peak shifts.

Table 1 XPS peak parameters for the V2p and Pt $4p_{3/2}$

	$4p_{3/2}$ (eV) (FWHM = 4.0)	$V2p_{3/2}$ (eV)	FWHM	$V2p_{1/2}$ (eV)	FWHM
Pt	519.5				
V_2O_3	—	515.3	3.4	522.7	3.5
VO_2	—	515.9	2.8	523.1	3.5
V_2O_5	—	516.8	2.2	523.8	3.2

Conclusions

Ordered thin films of vanadium oxide were grown on the Pt(111) surface and characterized in detail using AES, LEED, HREELS, LEIS, XPS and IRAS. The results demonstrate a layer-by-layer growth up to three monolayers. Isolated O═VO_x(x = 0–3) species form at submonolayer characteristic of a strong V═O loss feature at 128 meV, which bond weakly on the surface. Such isolated species condense into the 2D surface V_2O_3 domains upon coadsorption with CO at room temperature or annealing in UHV. A 2D surface V_2O_3 forms at 1 ML exhibiting a single phonon at 69 meV, which is stable upon annealing. A bilayer structure characteristic of 62 meV phonon loss forms at 2 ML. Further increasing the VO_x coverage high than 2 ML, results in attachment of the third layer with O═VO_x(x = 0–3) onto the bilayer structure. Such stacking structure is unstable, and desorbed from the bilayer surface upon annealing above 673 K. Under UHV conditions, the VO_x films are stable at V^{3+}. A higher oxidation state can be reached by oxidation at 'high pressure' of O_2, as evidenced by binding energy shifts in XPS and the appearance of $\nu_{V=O}$ in IRAS.

Acknowledgements

We gratefully acknowledge support for this work from the National Basic Research Program of China (973 program: 2010CB732303, 2013CB933102), the Major Project of the Chinese Ministry of Education (No: 309019), the National Natural Science Foundation of China (21033006, 21073149, 20923004, 21273178), the Program for Changjiang Scholars and Innovative Research Team in Universities (No. IRT1036), and the PhD Programs Foundation of the Chinese Ministry of Education (No. 20110121110010).

References

1 M. G. Ramsey, S. Surnev and F. P. Netzer, *Prog. Surf. Sci.*, 2003, **73**, 117–165.
2 K. Hermann and M. Witko, *Chem. Phys. Solid Surf.*, 2001, **9**, 136–198.
3 A. C. Dupuis, M. Abu Hija, B. Richter, H. Kuhlenbeck and H. J. reund, *Surf. Sci.*, 2003, **539**, 99–112.
4 M. Abu Haija, S. Guimond, Y. Romanyshyn, A. Uhl, H. Kuhlenbeck, T. K. Todorova, M. V. Ganduglia-Pirovano, J. Dobler, J. Sauer and H. J. Freund, *Surf. Sci.*, 2006, **600**, 1497–1503.
5 F. Stavale, H. Niehus and C. A. Achete, *Surf. Sci.*, 2009, **603**, 2721–2724.
6 N. Magg, B. Immaraporn, J. B. Giorgi, T. Schroeder, M. Bäumer, J. Döbler, Z. Wu, E. Kondratenko, M. Cherian, M. Baerns, P. C. Stair, J. Sauer and H. J. Freund, *J. Catal.*, 2004, **226**, 88–100.
7 N. Magg, J. B. Giorgi, T. Schroeder, M. Baumer and H. J. Freund, *J. Phys. Chem. B*, 2002, **106**, 8756–8761.

8 J. Schoiswohl, G. Kresse, S. Surnev, M. Sock, M. G. Ramsey and F. P. Netzer, *Phys. Rev. Lett.*, 2004, **92**, 206103–206106.
9 E. A. Kröger, D. I. Sayago, F. Allegretti, M. J. Knight, M. Polcik, W. Unterberger, T. J. Lerotholi, K. A. Hogan, C. L. A. Lamont and D. P. Woodruff, *Surf. Sci.*, 2007, **601**, 3350–3360; E. A. Kröger, D. I. Sayago, F. Allegretti, M. J. Knight, M. Polcik, W. Unterberger, T. J. Lerotholi, K. A. Hogan, C. L. A. Lamont and D. P. Woodruff, *Surf. Sci.*, 2008, **602**, 1267–1279.
10 M. S. Chen, W. Z. Weng and H. L. Wan, *J. Mol. Catal.*, 2000, **14**, 6–10.
11 C. Kolczewski, K. Hermann, S. Gulmond, H. Kuhlenbeck and H. J. Freund, *Surf. Sci.*, 2007, **601**, 5394–5402.
12 G. Kresse, S. Surnev, J. Schoiswohl and F. P. Netzer, *Surf. Sci.*, 2004, **555**, 118–134.
13 W. Xiao, K. Xie, Q. L. Guo and E. G. Wang, *J. Phys. Chem. B*, 2002, **106**, 4721–4724; W. Xiao, K. Xie, Q. L. Guo and E. G. Wang, *J. Phys.: Condens. Matter*, 2002, **14**, 6321–6328.
14 X. Rozanska and J. Sauer, *J. Phys. Chem. A*, 2009, **113**, 11586–11594.
15 O. R. Evans, A. T. Bell and T. Don Tilley, *J. Catal.*, 2004, **226**, 292–300.
16 H. Berndt, A. Martin, A. Brückner, E. Schreier, D. Müller, H. Kosslick, G. U. Wolf and B. Lücke, *J. Catal.*, 2000, **191**, 384–400.
17 A. Christodoulakis, M. Machli, A. A. Lemonidou and S. Boghosian, *J. Catal.*, 2004, **222**, 293–306.
18 J. L. Bronkema and A. T. Bell, *J. Phys. Chem. C*, 2007, **111**, 420–430.
19 W. C. Vining, A. Goodrow, J. Strunk and A. T. Bell, *J. Catal.*, 2010, **270**, 163–171.
20 W. C. Vining, J. Strunk and A. T. Bell, *J. Catal.*, 2011, **281**, 222–230.
21 H. L. Abbott, A. Uhl, M. Baron, Y. Lei, R. J. Meyer, D. J. Stacchiola, O. Bondarchuk, S. Shaikhutdinov and H. J. Freund, *J. Catal.*, 2010, **272**, 82–91.
22 E. A. Mamedov and V. C. Corberan, *Appl. Catal., A*, 1995, **127**, 1–40.
23 I. Giakoumelou, R. M. Caraba, V. I. Parvulescu and S. Boghosian, *Catal. Lett.*, 2002, **78**, 209–214.
24 I. Giakoumelou, C. Fountzoula, C. Kordulis and S. Boghosian, *J. Catal.*, 2006, **239**, 1–12.
25 Y. Segura, L. Chmielarz, P. Kustrowski, P. Cool, R. Dziembaj and E. F. Vansant, *J. Phys. Chem. B*, 2006, **110**, 948–955.
26 M. D. Negra, M. Sambi and G. Granozzi, *Surf. Sci.*, 1999, **436**, 227–236.
27 Q. Guo, S. Lee and D. W. Goodman, *Surf. Sci.*, 1999, **437**, 38–48.
28 G. S. Wong, D. D. Kragten and J. M. Vohs, *Surf. Sci.*, 2000, **452**, L293–L297; G. S. Wong, D. D. Kragten and J. M. Vohs, *J. Phys. Chem. B*, 2001, **105**, 1366–1373.
29 W. Gao, C. M. Wang, H. Q. Wang, V. E. Henrich and E. I. Altman, *Surf. Sci.*, 2004, **559**, 201–213.
30 E. A. Kröger, F. Allegretti, M. J. Knight, M. Polcik, D. I. Sayago, D. P. Woodruff and V. R. Dhanak, *Surf. Sci.*, 2006, **600**, 4813–4824.
31 V. Brazdova, M. V. Ganduglia-Pirovano and J. Sauer, *J. Phys. Chem. B*, 2005, **109**, 23532–23542.
32 N. Magg, J. B. Giorgi, M. M. Frank, B. Immaraporn, T. Schroeder, M. Baumer and H. J. Freund, *J. Am. Chem. Soc.*, 2004, **126**, 3616–3626.
33 G. S. Wong and J. M. Vohs, *Surf. Sci.*, 2002, **498**, 266–274.
34 C. Popa, M. Veronica, G. Pirovano and J. Sauer, *J. Phys. Chem. C*, 2011, **115**, 7399.
35 M. V. Ganduglia-Pirovano, C. Popa, J. Sauer, H. Abbott, A. Uhl, D. Stacchiola, O. Bondarchuk, S. Shaikhutdinov and H. J. Freund, *J. Am. Chem. Soc.*, 2010, **132**, 2345–2349.
36 Z. Wu, A. J. Rondinone, I. N. Ivanov and S. H. Overbury, *J. Phys. Chem. C*, 2011, **115**, 25368–25378.
37 K. B. Lewis, S. T. Oyama and G. A. Somorjai, *Surf. Sci.*, 1990, **133**, 75–83.
38 K. Kishi and K. Fujiwara, *J. Electron Spectrosc. Relat. Phenom.*, 1995, **71**, 51–59; K. Kishi and K. Fujiwara, *J. Electron Spectrosc. Relat. Phenom.*, 1997, **85**, 123–134.
39 M. A. Haija, A. Bandara, F. Hobel, H. Kuhlenbeck, G. Rupprechter and H. J. Freund, *Top. Catal.*, 2007, **46**, 223–230.
40 S. Guimond, J. M. Sturm, D. Gobke, Y. Romanyshyn, M. Naschitzki, H. Kuhlenbeck and H. J. Freund, *J. Phys. Chem. C*, 2008, **112**, 11835–11846.
41 J. M. Sturm, D. Gobke, H. Kuhlenbeck, J. Dobler, U. Reinhardt, M. V. Ganduglia-Pirovano, J. Sauer and H. J. Freund, *Phys. Chem. Chem. Phys.*, 2009, **11**, 3290–3299.
42 C. Klein, G. Kresse, S. Surnev, F. P. Netzer, M. Schmid and P. Varga, *Phys. Rev. B: Condens. Matter*, 2003, **68**, 235416–235426.
43 G. Kresse, S. Surnev, M. G. Ramsey and F. P. Netzer, *Surf. Sci.*, 2001, **492**, 329–344; G. Kresse, S. Surnev, M. G. Ramsey and F. P. Netzer, *Surf. Sci.*, 2001, **495**, 91–106.
44 S. Surnev, G. Kresse, M. G. Ramsey and F. P. Netzer, *Phys. Rev. Lett.*, 2001, **87**, 086102–086106.
45 S. Surnev, L. Vitali, M. G. Ramsey, F. P. Netzer, G. Kresse and J. Hafner, *Phys. Rev. B: Condens. Matter*, 2000, **61**, 13945–13954.
46 M. Sambi, M. Petukhov, B. Domenichini, G. A. Rizzi, S. Surnev, G. Kresse, F. P. Netzer and G. Granozzi, *Surf. Sci.*, 2003, **529**, L234–L238.
47 J. Schoiswohl, M. Sock, Q. Chen, G. Thornton, G. Kresse, M. G. Ramsey, S. Surnev and F. P. Netzer, *Top. Catal.*, 2007, **46**, 137–149.
48 J. Schoiswohl, M. Sock, S. Eck, S. Surnev, M. G. Ramsey, F. P. Netzer and G. Kresse, *Phys. Rev. B: Condens. Matter Mater. Phys.*, 2004, **69**, 155403–155419.
49 J. Schoiswohl, M. Sock, S. Surnev, M. G. Ramsey, F. P. Netzer, G. Kresse and J. N. Andersen, *Surf. Sci.*, 2004, **555**, 101–117.
50 J. Schoiswohl, S. Eck, M. G. Ramsey, J. N. Andersen, S. Surnev and F. P. Netzer, *Surf. Sci.*, 2005, **580**, 122–136.
51 J. Schoiswohl, S. Surnev, M. Sock, S. Eck, M. G. Ramsey, F. P. Netzer and G. Kresse, *Phys. Rev. B: Condens. Matter Mater. Phys.*, 2005, **71**, 165437–165445.

52 M. Petukhov, G. A. Rizzi and G. Granozzi, *Surf. Sci.*, 2001, **490**, 376–384; M. Petukhov, G. A. Rizzi and G. Granozzi, *Thin Solid Films*, 2001, **400**, 154–159.
53 H. H. Brongersma and T. M. Buck, *Nucl. Instrum. Methods*, 1978, **149**, 569–575.
54 P. J. Feibelman, S. Esch and T. Michely, *Phys. Rev. Lett.*, 1996, **77**, 2257–2260.
55 Q. Fu, W. X. Li, Y. X. Yao, H. Y. Liu, H. Y. Su, D. Ma, X. K. Gu, L. M. Chen, Z. Wang, H. Zhuang, B. Wang and X. H. Bao, *Science*, 2010, **328**, 1141–1144.
56 H. Hopster and H. Ibach, *Surf. Sci.*, 1978, **77**, 109–117.
57 F. Sedona, G. A. Rizzi, S. Agnoli, F. X. L. Xamena, A. Papageorgiou, D. Ostermann, M. Sambi, P. Finetti, K. Schierbaum and G. Grano zzi, *J. Phys. Chem. B*, 2005, **109**, 24411–24426.
58 S. R. G. Carrazán, P. J. Benítez and V. Rives, *Vib. Spectrosc.*, 1993, **5**, 295.
59 S. Guimond, M. Abu Haija, S. Kaya, J. Lu, J. Weissenrieder, S. Shaikhutdinov, H. Kuhlenbeck, H. J. Freund, J. Döbler and J. Sauer, *Top. Catal.*, 2006, **38**, 117–125.
60 B. Tepper, B. Richter, A. C. Dupuis, H. Kuhlenbeck, C. Hucho, P. Schilbe, M. A. bin Yarmo and H. J. Freund, *Surf. Sci.*, 2002, **496**, 64–72.
61 E. Hryha, E. Rutqvist and L. Nyborg, *Surf. Interface Anal.*, 2012, **44**, 1022–1025.
62 S. Surnev, M. G. Ramsey and F. P. Netzer, *Prog. Surf. Sci.*, 2003, **73**, 117–165.
63 M. Tischer, L. Tröger, H. Klein, R. Domesle, E. S. Lox, G. Prescher and P. Albers, *Phys. Chem. Chem. Phys.*, 1999, **1**, 2815–2823.
64 G. A. Sawatzky and D. Post, *Phys. Rev. B*, 1979, **20**, 1546–1520.
65 M. Baron, H. Abbott, O. Bondarchuk, D. Stacchiola, A. Uhl, S. Shaikhutdinov and J. Sauer, *Angew. Chem.*, 2009, **121**, 8150–8153.